9-4-2008

Lateral Circulation and Suspended Sediment Transport in a Curved Estuarine Channel: Winyah Bay, SC, USA

Yong Hoon Kim
University of South Carolina - Columbia

George Voulgaris
University of South Carolina - Columbia, gvoulgaris@geol.sc.edu

Publication Info

Published in *Journal of Geophysical Research*, Volume 113, Issue C09006, 2008, pages 1-15.
Kim, Y. H. & Voulgaris, G. (2008). Lateral circulation and suspended sediment transport in a curved estuarine channel: Winyah Bay, SC, USA. *Journal of Geophysical Research, 113* (C09006), 1-15.

Lateral circulation and suspended sediment transport in a curved estuarine channel: Winyah Bay, SC, USA

Yong Hoon Kim[1,2] and George Voulgaris[2]

Received 17 August 2007; revised 14 May 2008; accepted 9 June 2008; published 4 September 2008.

[1] Shipborne vertical profiles of flow and suspended sediment concentration collected on a transect, across a curved, nonsymmetrical estuarine channel are presented. Analysis of the transient cross-channel momentum balance equation shows that the lateral circulation pattern is controlled by the interaction between centrifugal and lateral baroclinic forcings although those two might not be necessarily in balance as suggested earlier by Seim and Gregg (1997). Instead, differential along-channel advection and local acceleration appear to influence greatly lateral circulation dynamics. During ebb when the water column is highly stratified, the interaction between centrifugal acceleration and opposite-directed lateral baroclinic forcing results in weak lateral flows. During flood, lateral flows are dominated by centrifugal acceleration, which is directed toward the outside of the curvature at the mid-depth because of the nonlogarithmic current profile, and reinforced by lateral baroclinic forcing. This results in strong two-layer clockwise circulation (looking up-estuary) during flood. The eastward-directed bottom currents during ebb deliver only a small amount of suspended sediment from the relatively narrow western shoal to the channel bed. During flood, the west-directed near-bed currents deliver a significant amount of sediments from the gentle, broad eastern shoal, which in conjunction with the locally resuspended sediment load promotes the development of the estuarine turbidity maximum. Increased lateral advection of sediments during flood reinforces a tidal asymmetry in the development of turbidity maximum. Decomposition analysis of lateral sediment fluxes averaged over a tidal cycle suggests convergence of sediment toward the center of the channel is driven mainly by the oscillatory tidal component.

Citation: Kim, Y. H., and G. Voulgaris (2008), Lateral circulation and suspended sediment transport in a curved estuarine channel: Winyah Bay, SC, USA, *J. Geophys. Res.*, *113*, C09006, doi:10.1029/2007JC004509.

1. Introduction

[2] Estuaries are coastal environments influenced by both riverine and marine processes that include sediment discharge from rivers, mixing of fresh and salt waters, and the influence of tides. Within these environments high levels of suspended sediment concentrations are encountered and their trapping is controlled by hydrodynamic (i.e., tidal dynamics, river discharge, salinity stratification, and residual flow patterns) and sedimentary (i.e., size, flocculation processes etc) characteristics.

[3] The majority of sediment trapping occurs at the turbidity maximum, a region usually found in the upper or middle reaches of an estuary, which is defined as the location where sediment concentrations are larger than those found upstream or downstream [*Nichols and Biggs*, 1985; *Grabemann and Krause*, 1989]. Traditionally, the location of the turbidity maximum has been attributed to the convergence of riverine surface flow and landward-directed residual bottom flow at the landward limit of the salt intrusion [*Dyer*, 1986]. However these elevated sediment concentrations can also be attributed to locally induced resuspension of fine sediments from the bed during times of increased tidal current velocity creating a turbidity maximum seaward of the salt intrusion [e.g., *Allen et al.*, 1980; *Nichols and Biggs*, 1985]. Furthermore, a turbidity maximum can be observed landward of the salt intrusion because of the barotropic tidal asymmetry [*Friedrichs et al.*, 1998].

[4] In addition to along-channel flows, it has been recognized that, despite their smaller intensities, lateral flows may play a significant role in momentum balance, mixing of salt and other scalars, and transport of particles [*Dronkers*, 1996; *Chant and Wilson*, 1997; *Seim and Gregg*, 1997; *Geyer et al.*, 1998; *Lacy and Monismith*, 2001; *Lerczak and Geyer*; 2004; *Huijts et al.*, 2006]. Numerical simulations by *Lerczak and Geyer* [2004] showed that lateral circulation significantly influences both the along- and cross-channel momentum budget and that lateral advection can even act as a driving term for estuarine exchange flow in the tidally averaged, along-channel momentum balance.

[1]Now at Horn Point Laboratory, University of Maryland Center for Environmental Science, Cambridge, Maryland, USA.
[2]Department of Geological Sciences, Marine Science Program, University of South Carolina, Columbia, South Carolina, USA.

0148-0227/08/2007JC004509

[5] In general, lateral (also known as transverse, secondary, or cross-channel) flows in estuaries have been attributed to a variety of mechanisms that include centrifugal forcing due to channel curvature [e.g., *Kalkwijk and Booij*, 1986; *Geyer*, 1993; *Chant and Wilson*, 1997; *Seim and Gregg*, 1997; *Chant*, 2002; *Lacy and Monismith*, 2001], Coriolis forcing [e.g., *Ott and Garrett*, 1998], cross-channel density gradient [e.g., *Smith*, 1976; 1980; *Nunes Vaz and Simpson*, 1985; *Dronkers*, 1996; *Lerczak and Geyer*, 2004] and lateral bathymetric variability [e.g., *Li and O'Donnell*, 1997; *Valle-Levinson et al.*, 2000]. In most estuarine environments, the mechanisms listed above can reinforce or compete with each other. Especially for a curved channel, the analytical solution presented by *Kalkwijk and Booij* [1986] underlines the importance of centrifugal forcing in lateral circulation processes. Furthermore, vertical stratification in a curved estuarine channel can contribute to a lateral salinity gradient that can also drive lateral flow [*Dronkers*, 1996; *Chant and Wilson*, 1997; *Seim and Gregg*, 1997; *Lacy and Monismith*, 2001]. This lateral baroclinic pressure gradient may reinforce, balance or oppose the curvature-induced flow. *Chant and Wilson* [1997] presented observations showing along-channel variation in the relative dominance of centrifugal and lateral baroclinic forcings. *Seim and Gregg* [1997] proposed a Froude number as a criterion of the balance between centrifugal and baroclinic forcings. *Lacy and Monismith* [2001] suggested that a time-varying balance between centrifugal acceleration and baroclinic pressure gradient produces lateral circulation in clockwise and counterclockwise directions depending on tidal stage.

[6] The majority of the work on lateral estuarine circulation has focused on circulation patterns with limited or no attention to sediment transport processes. Studies on lateral sediment transport have focused predominantly on rather straight estuarine channels. For example, *Geyer et al.* [1998] used a numerical simulation to show that trapping of fine-grained sediments on the shallow areas of a straight estuarine channel is due to the lateral advection of sediments from the deeper channel to the shoal regions. Most recently, *Huijts et al.* [2006] used perturbation analysis, in an idealized straight estuarine channel, to show that lateral density gradient is more important than Coriolis in distributing sediment laterally. It was also suggested that when frictional forces are small, sediment tends to accumulate on the right-hand side bank (when looking up-estuary in the northern hemisphere) in response to Coriolis forcing, while under moderate or high frictional forcing sediment accumulation occurs on the side of the estuary where the water is less saline. *Fugate et al.* [2007] reported tidal asymmetries in lateral circulation, stratification, and resuspension resulting in net sediment flux on the eastern side of the upper part of Chesapeake Bay estuary, which is also straight channel system. Limited experimental or theoretical work exists showing the effect of channel curvature on lateral sediment transport.

[7] The objective of this study is to unravel the interaction of lateral flow, sediment transport and trapping for Winyah Bay (South Carolina, USA), a partially mixed, curved estuary. Field experimental results are presented on the development of lateral flow and sediment fluxes both in the along and cross-channel directions. Momentum balance analysis is used to elucidate the interaction between centrifugal, Coriolis, and lateral baroclinic pressure gradient forces on lateral flows. Further, tidal decomposition analysis of suspended sediment fluxes is used to identify the relative contribution of residual advective and oscillatory tidal components in both along-channel and lateral fluxes. The implication of lateral sediment flux on the development of turbidity maximum is also discussed.

2. Study Area and Data Analysis

[8] Winyah Bay, South Carolina (see Figure 1) is one of the largest estuarine systems on the eastern coast of the U.S. The estuary is 29 km long and encompasses a total area of 157 km^2 [*South Carolina Sea Grant Consortium*, 1992]. It is subjected to semidiurnal tidal forcing with a mean tidal range of 1.4 m at the mouth and 1.0 m at the Sampit River entrance, some 30 km upstream [*NOS*, 1995]. The annual mean freshwater input to the estuary is approximately 557 $m^3\ s^{-1}$ and is derived from a drainage area of 47,060 km^2 [*Patchineelam*, 1999].

[9] Winyah Bay is a partially mixed estuary with an along-estuary salinity gradient of approximately 1 psu km^{-1} [*Ramsey*, 2000]. The location of the salt front depends on freshwater discharge; during periods of high river discharge the front is located near the mouth of the estuary, while during periods of low discharge the salt wedge reaches distances up to 55 km upstream [*South Carolina Sea Grant Consortium*, 1992]. The average depth of the bay is 4.2 m, with an artificially maintained shipping channel of 8.2 m depth. To the east of the estuary an extensive shallow (<0.5 m at low tide) flat area exists fringed by extensive intertidal mud flat areas (Figure 1).

[10] The estuary has a complex morphology with a single channel in the upper and lower reaches and a bifurcated channel system (main and western channels respectively) in the middle part of the estuary. The channel junctions are located in the northern and southern ends of the middle estuary. The channels at these junction points are gently curved in opposite directions; westward and eastward for the northern and southern junctions, respectively (see Figure 1). *Kim and Voulgaris* [2005] showed that the presence of the bifurcated channels in the middle part of the estuary modifies the typical gravitational circulation; it creates a near-bed landward-directed residual flow that is stronger in the deeper main than the shallower western channel.

[11] Experimental work [*Ramsey*, 2000; *Kim and Voulgaris*, 2003; *Kim*, 2006] has shown that the zone of high concentration of suspended sediments (i.e., estuarine turbidity maximum, ETM) is located in the vicinity of the east (i.e., right when looking up-estuary) curved section near the northern junction and this is the main focus area in this study (Figure 1). The radius of the curvature at this location was calculated using the method described in *Chant and Wilson* [1997] and was found to be approximately 3000 m [*Kim*, 2006].

[12] A 1-km-long transverse section (transect A in Figure 1), with a nonsymmetric bathymetric profile, was surveyed for a tidal cycle. Continuous mapping of the three-dimensional current structure along the transect was carried out using a ship-mounted, downward-looking RDI acoustic Doppler current profiler (ADCP, 1200 KHz) during July 2004. A total of 58 survey loops were conducted during a period of

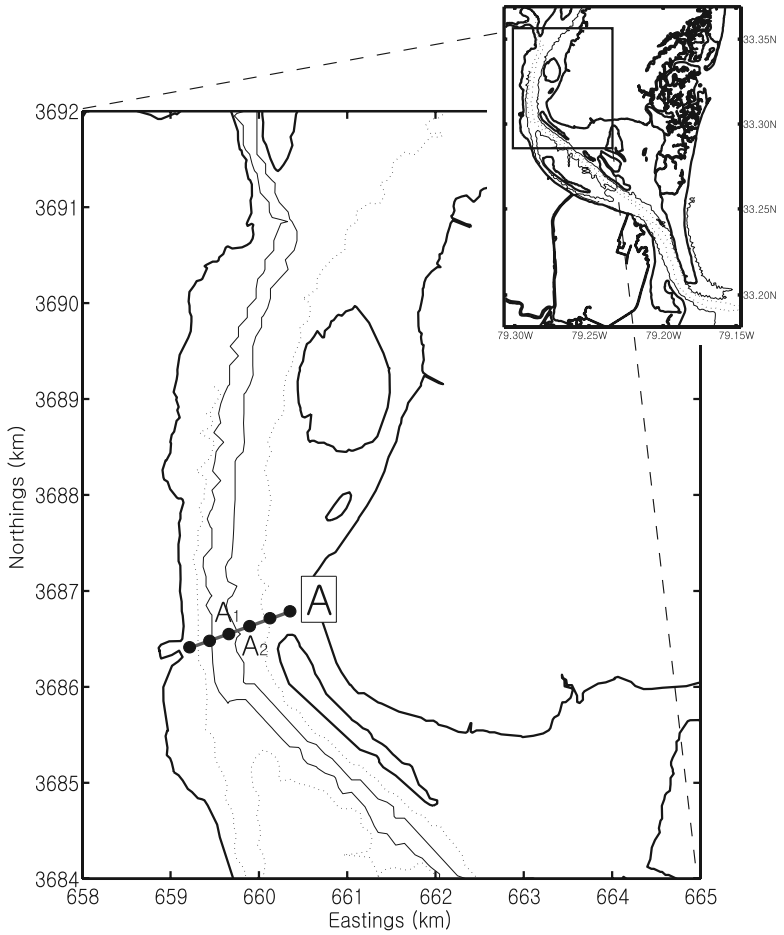

Figure 1. Study area map. Transect A indicates the cross-section investigated in this study. Black circles on the transect indicate CTD stations. Station A_1 and A_2 represents the location of collection of the data shown in Figures 2 and 3, respectively. Solid and dashed lines represent 3.5 m and 6.5 m bathymetric contours. Inset shows the whole area of Winyah Bay.

12.5 hours. Bottom-tracking correction was carried out using data from an on-board differential GPS system. The first bin of the ADCP was located at 0.9 m below the water surface and the size of each bin was 0.25 m. One-second instantaneous current data were recorded and later averaged to 10-second mean velocities.

[13] Temporally averaged currents from each bin were decomposed into along- and cross-channel components based on the local orientation of the major flow direction derived from principal component analysis (i.e., curvilinear coordinate system). The derived cross-channel direction was also reconfirmed making sure that this direction resulted in a minimum variance in the cross-channel flow. Positive sign represents up-estuary (i.e., north, northeast or direction of flood) and east or northeast (i.e., right when looking up-estuary) directed flows in the along- and cross-channel axes, respectively.

[14] Vertical profiles of temperature, salinity and suspended sediment concentration were also taken at six locations (200 m apart) along the transect (Figure 1) using an Ocean Sensors 200 CTD and an integrated optical backscatterance sensor (OBS-3, D&A Instruments). The data were collected at 1 Hz corresponding to a vertical resolution of approximately 2.5 cm. The OBS signal was later converted to sediment mass concentration using a calibration equation developed from the analysis of filtered water samples [*Kim*, 2006]. Sea surface variation during the experimental period was measured at 6 minute interval using a self-recording pressure gauge (RBR, XR-420 TG) that was installed at the eastern end of transect A (see Figure 1). Similar pressure data were also collected at the western end of the transect using a bottom-mounted Nortek Aquadopp (2 MHz) current profiler every 10 minutes.

[15] Sediment concentration estimates from the calibrated OBS sensors were used to develop a calibration constant for the acoustic intensity of the backscattered data recorded by the ADCP. Using this constant the acoustic backscatter data from the ADCP were converted to suspended sediment concentration based on the method described in *Kim and Voulgaris* [2003] and *Kim* [2006]. This analysis provided concentration data with the same spatial and temporal resolution as the flow data. The product of the cross-channel component of current and sediment concentration was used to estimate instantaneous lateral sediment fluxes. The fluxes were subsequently averaged over the semidiurnal tidal cycle. Assuming that velocity and concentrations consist of a mean and a tidal component, the tidally averaged fluxes

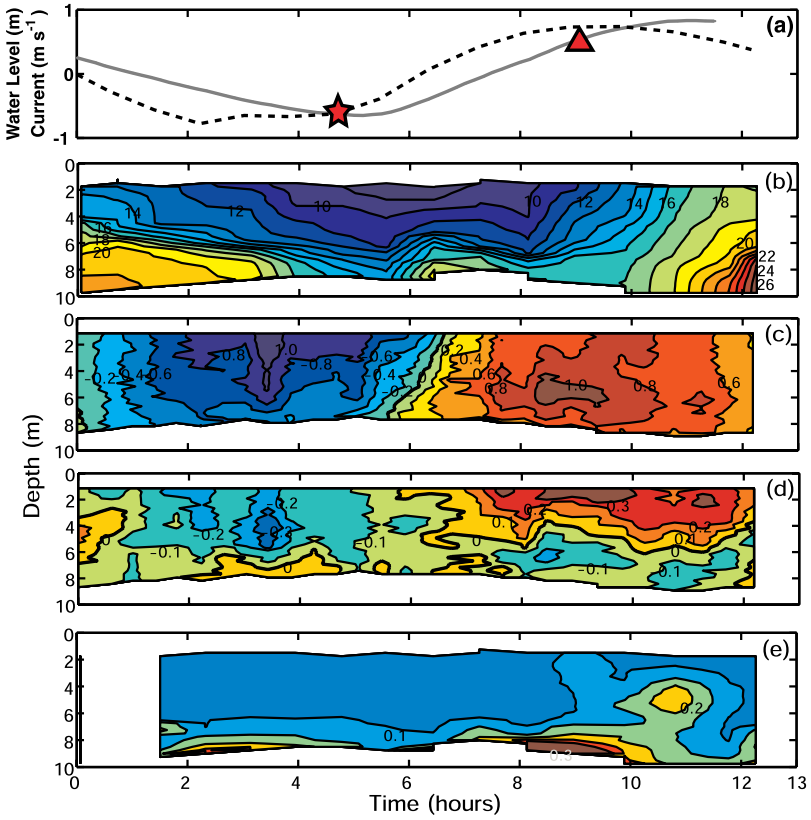

Figure 2. Time series of data collected in the middle of the channel (A_1; see Figure 1 for location). (a) Water level at the western margin of the channel (gray solid line) and depth-averaged along-channel velocity (dashed line); (b) salinity (in psu); (c) along-channel current velocity (in m s^{-1}); (d) lateral current velocity in m s^{-1}; (e) OBS-derived suspended sediment concentration in (kg m^{-3}). Positive sign in along- and cross-channel velocities represents northward (i.e., up-estuary) and eastward (i.e., rightward when looking up-estuary) direction, respectively. Thick solid contour lines denote zero velocity. White area represents no data due to instrument malfunction. Star and triangle symbols in (a) represent times for transects in Figures 4 and 5, respectively.

were decomposed into residual advective and tidal components as follows:

$$\langle V(x,t)\cdot C(x,t)\rangle = \langle V(x,t)\rangle\cdot\langle C(x,t)\rangle + \langle \tilde{V}(x,t)\cdot\tilde{C}(x,t)\rangle \quad (1)$$

where V and C represent the magnitude of lateral flow and suspended sediment concentration as a function of location (x) and time (t) along the transect as provided by the ADCP data; the brackets denote tidally averaged quantities, and the tilde is for the oscillatory tidal component. Residual and tidal components of the cross-channel currents were estimated using a least-squares method that fits the raw data to the dominant tidal period (semidiurnal) for the study site [*Kim and Voulgaris*, 2005]. Suspended sediment concentrations are also decomposed into tidal and mean components, respectively. First the tidal mean value was calculated and then the oscillatory component was evaluated as the difference between the instantaneous and the tidally averaged concentration.

3. Results

[16] This section consists of two parts. In the first part the data on water level, currents, salinity, and suspended sediment concentration are presented in terms of temporal and spatial variability, while the second part presents the results on sediment transport in the along- and cross-channel directions, respectively.

3.1. Temporal Variability

[17] Time-series of hydrodynamic, hydrographic and sediment concentration data collected at two locations A_1 and A_2 (see Figure 1) located in the middle and the eastern margin of the channel, are shown in Figures 2 and 3. Data collection started at the early stage of ebb and ended at high slack water, as demonstrated in Figure 2a. Thus the first 6 hours of data represent ebb conditions while the remainder is representative of flood tidal conditions.

3.1.1. Salinity

[18] The salinity at both stations exhibits a tidal variability with values ranging from 8 psu (at the surface during low water) to 20 and 26 psu near the bed at high water in the main channel (Figure 2b) and shoal (Figure 3b), respectively. In the center of the channel, a strong halocline with a vertical gradient of approximately 3 psu m^{-1} is observed at 6 m below the sea surface especially during the ebb and early flood (hours 0 to 8), indicating strong stratification. The halocline is also present on the shoal during early-to-mid ebb.

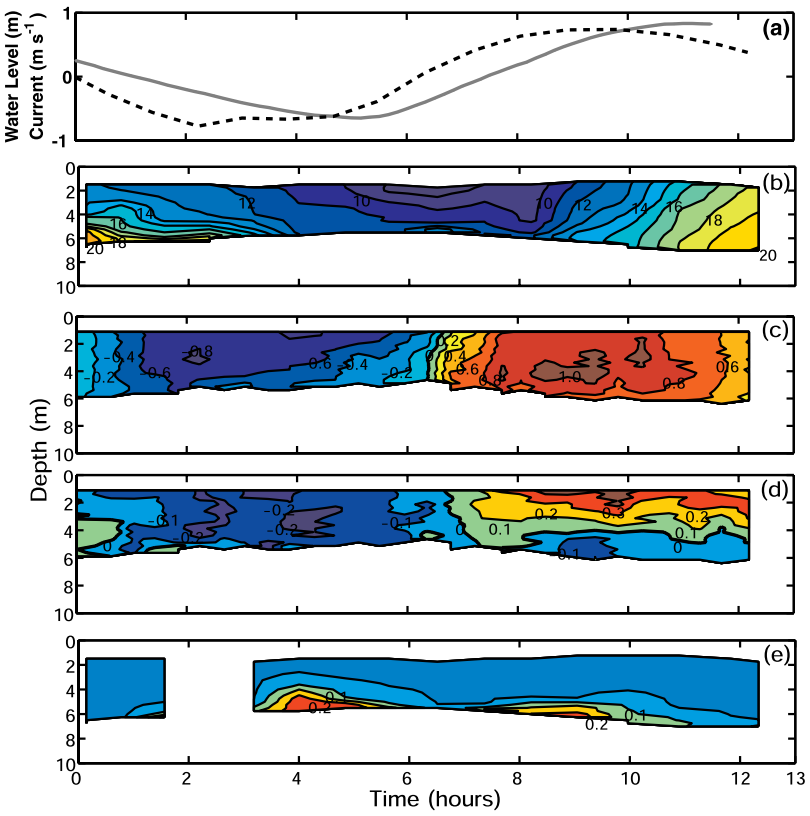

Figure 3. Time series of data collected on the shoal station (A_2; see Figure 1 for location). (a) Water level at the western margin of the channel (gray solid line) and depth-averaged along-channel velocity (dashed line); (b) salinity (in psu); (c) along-channel current velocity (in m s^{-1}); (d) lateral current velocity in m s^{-1}; (e) OBS-derived suspended sediment concentration in (kg m^{-3}). Positive sign in along- and cross-channel velocities represents northward (i.e., up-estuary) and eastward (i.e., rightward when looking up-estuary) direction, respectively. Thick solid contour lines denote zero velocity.

This halocline is observed at the same depth (6 m) as in the channel, which corresponds to the bottom layer of the shoal (Figures 2b and 3b). During the maximum and late stages of flood (hours 9 to 12), the water is well mixed with top-to-bottom salinity differences of only 2–3 psu for both the channel and shoal locations. Overall, the time-series indicate that tidal asymmetry in stratification pattern is significant in both locations and presumably throughout the whole transect.

3.1.2. Along-Channel and Lateral Flows

[19] Along-channel current velocities in the channel reach up to 1.2 and 1.0 m s^{-1} during ebb and flood, respectively (Figure 2c). During ebb, maximum velocity is observed in the surface layer and decreases gradually to the bed indicating a frictional logarithmic velocity profile. On the other hand, during flood the maximum along-channel current speed is observed below mid-depth at approximately 6m below the sea surface and 2m above the bed (Figure 2c). This mid-depth layer of maximum flood velocity is also observed at approximately 2/3 of the water depth (~4–5 m below the surface) on the shoal (Figure 3c). While the magnitude of the maximum flood current over the shoal is similar to that measured in the channel (~1 m s^{-1}), maximum ebb flow speed is smaller reaching only 0.8 m s^{-1} (Figure 2c).

[20] During ebb, lateral flow is mostly directed toward the west (i.e., toward the outside of the curvature) in the surface to middle layers of the channel (Figure 2d). It reaches a maximum value of 0.3 m s^{-1}, which is approximately 30% of the observed along-channel flow. A three layer current structure is developed during the early stage of ebb (hours 0 to 1; Figure 2d). Then, a two-layer counterclockwise flow (westward- and eastward-directed flow in the surface and bottom layers, respectively) is present during the middle to late ebb (Figure 2d, hours 2.5 to 5), while an opposite-directed (i.e., clockwise) two-layered flow is present during the whole period of flood (hours 6 to 12). The lateral flow on the shoal is directed to the outside of the curvature (i.e., westward) throughout the water column during most of ebb, which is consistent to that observed in the surface and middle layers of the channel but its magnitude does not exceed 0.25 m s^{-1} (Figure 3d). During flood, the eastward-directed surface flow in the channel reaches values of up to 0.3 m s^{-1}, while the bottom flow obtains values not exceeding 0.2 m s^{-1} (Figure 2d). On the shoal, a similar two-layered lateral flow is observed but it is present only during mid to late flood (hours 8 to 12, Figure 3d).

3.1.3. Sediment Concentration

[21] Suspended sediment concentrations measured with the OBS sensor are approximately 0.02 kg m^{-3} during slack

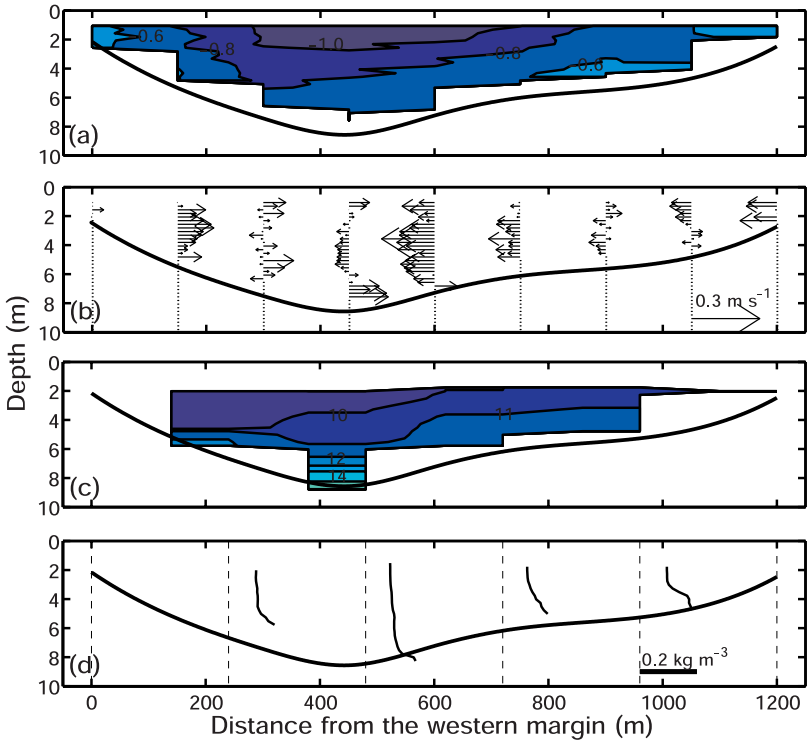

Figure 4. Vertical and along-transect variability of flow, salinity and suspended sediment concentration during maximum ebb (see star symbol in Figure 2a). (a) Contour map of along-channel current velocity (in m s^{-1}); (b) vectors of lateral currents; (c) lateral distribution of salinity (in psu); and (d) OBS-derived profiles of suspended sediment concentration.

water at both high and low tide, representing the ambient background levels for the study area. The concentration increases during both maximum ebb and flood in response to increasing flow speeds. Both the absolute concentration and the vertical distribution pattern of suspended sediments exhibit a strong tidal asymmetry with higher concentrations in the channel (up to 0.3 kg m^{-3}) during the flood. In general, sediments are advected/diffused upward from the bed during flood although it is worth noting that locally, slightly elevated concentration of sediments is observed at 4–6 m below the surface later in the flood (see hours 10–11; Figure 2e), which might be related to lateral advection as it is discussed later (see section 4.3). Overall, the observed tidal asymmetry in vertical sediment distribution seems to follow the stratification patterns observed during each tidal stage (see Figure 2b). Maximum observed sediment concentration on the shoal is 0.25 kg m^{-3}, which is slightly smaller than that found on the main channel. Although tidal asymmetry in the concentration is not prominent on the shoal, the vertical distribution pattern is distinctly different between ebb and flood. Although sediment resuspension is confined near the bed during flood, the sediments are diffused throughout the whole water column during ebb (Figure 3e), which is opposite of that observed in the channel.

3.2. Cross-Channel Variability

[22] Although a large number of transect data was collected during the experimental period, for brevity purposes only results from the maximum ebb and flood periods (hours 4 to 5 and 9 to 10, respectively) are presented in this section.

3.2.1. Along-Channel and Lateral Flows

[23] During ebb, the maximum along-channel velocity (1.2 m s^{-1}) is observed near the surface in the center of the channel. It decreases gradually toward the bed, exhibiting the structure of a typical vertical logarithmic velocity profile [e.g., *Dyer*, 1986]. The magnitude of the along-channel flow also decreases toward the channel margins (Figure 4a). Lateral flows (Figure 4b) exhibit cross-channel and vertical variability both in terms of magnitude and direction. Lateral flow is directed toward the east in the surface and bottom layers at the center of the channel (approximately 300–500 m from the western margin), while in the middle layer the flow is toward the west (i.e., three-layer structure). Lateral flow on the western and eastern bank is directed to the east and west, respectively, throughout the water column. This results in a lateral flow convergence in the surface and mid water layers at a location some 400 m from the western margin.

[24] Along-channel currents during flood reach a maximum velocity of 0.9 m s^{-1} at mid-depth in both sides of the main channel (i.e., approximately 300–400 and 600–1000 m from the western margin; Figure 5a). The occurrence of a mid-depth maximum flood flow is caused by the outflow of the fresh water in the surface layer, as commonly observed in estuaries [e.g., *Dyer*, 1986; *Jay and Musiak*, 1994]. In addition, the lateral advection of low momentum water from the western shoal to the center of channel contributes to the development of flow maxima at mid depth [e.g., *Lacy et al.*,

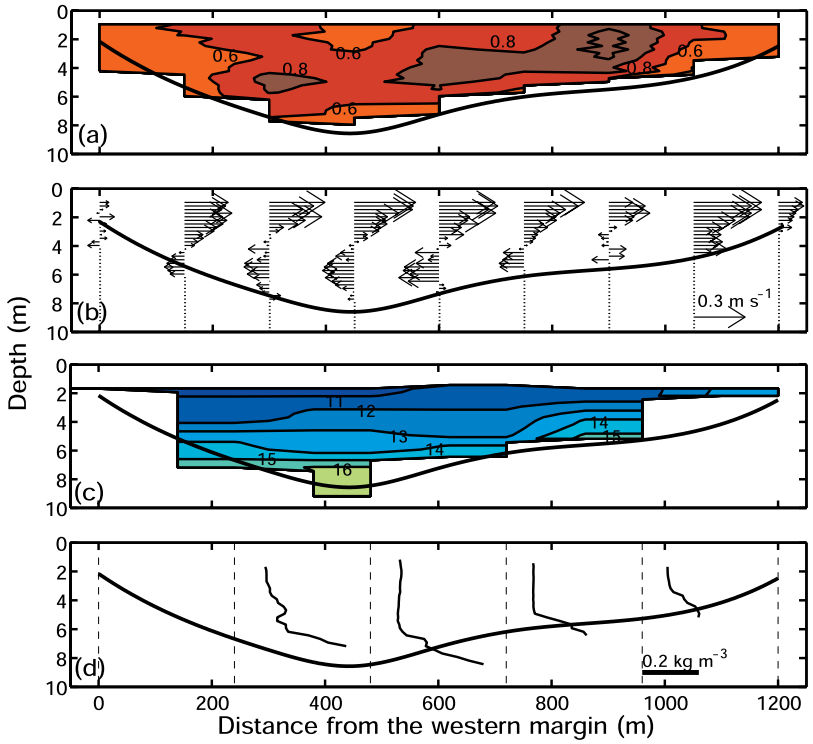

Figure 5. Vertical and along-transect variability of flow, salinity and suspended sediment concentration during maximum flood (see triangle symbol in Figure 2a). (a) Contour map of along-channel current velocity (in m s^{-1}); (b) vectors of lateral currents; (c) lateral distribution of salinity (in psu); and (d) OBS-derived profiles of suspended sediment concentration.

2003]. Lateral flows during flood are stronger and more consistent than during ebb (Figures 4b and 5b); they are directed to the east in the surface layer (from 0 to 4–5 m below the sea surface) with maximum speed of 0.3 m s^{-1} near the surface (Figure 5b) while the near-bed lateral currents are directed westward. This two-layer flow results in the development of a clockwise circulation pattern that is observed in both channel and shoals during the whole period of flood (see Figures 2c and 3c).

3.2.2. Salinity Variation

[25] During ebb the water mass in the center of the channel has lower salinity than that on the eastern shoal (Figure 4c). This is due to the combined effect of curvature-induced forcing toward the outside of curvature and the differential advection, i.e., the fresher water mass flows out faster in the channel than on the shoals [e.g., *Nunes Vaz and Simpson*, 1985; *Dronkers*, 1996]. This lateral structure of salinity leads to the development of a baroclinic pressure gradient directed toward the west during ebb. During flood the isohalines are mostly horizontal (Figure 5c) indicating a smaller role in the development of a lateral baroclinic forcing than during ebb.

3.2.3. Sediment Concentration

[26] Suspended sediment concentrations attain higher values (up to 0.30 g l^{-1}) during maximum flood than maximum ebb (up to 0.15 g l^{-1}; Figures 4d and 5d). The vertical profiles during ebb and flood generally show concentrations near the background level in the surface layer increasing toward the bed, resembling the form of a typical Rouse profile [*Blake et al.*, 2001; *Orton and Kineke*, 2001]. This implies that the observed suspended sediment concentrations are generally the result of local resuspension from the bed. As such the concentration is expected to be proportional to the strength of bottom shear. Lateral variation of suspended sediment concentration is such that higher concentrations occur in the center of the channel than over the adjacent shoals (Figure 5d). In some occasions though, elevated concentrations are observed at the mid-depth (4 to 6m) of the channel (see Figure 5d). Such local highs in concentration do not seem to be related to local benthic resuspension processes and it is hypothesized that it is the result of lateral advective processes.

3.3. Sediment Transport

3.3.1. Cross-Channel Sediment Transport

[27] In order to investigate the net contribution of lateral sediment transport, tidally averaged sediment fluxes are estimated for transect A using equation (1). Figure 6 shows the tidally averaged lateral currents and suspended sediment concentration, and the results of tidal decomposition of the lateral sedimentary fluxes along transect A. The residual advective flux in the surface layer (up to 2 m depth) is directed to the east while in the bottom layer is directed to the west (below 2 m water depth; Figure 6c). This leads to the creation of a two-layered clockwise residual advective sediment flux. The magnitude of westward-directed bottom fluxes is approximately 10 times larger than that of eastward-directed surface fluxes. The maximum tidal fluxes are

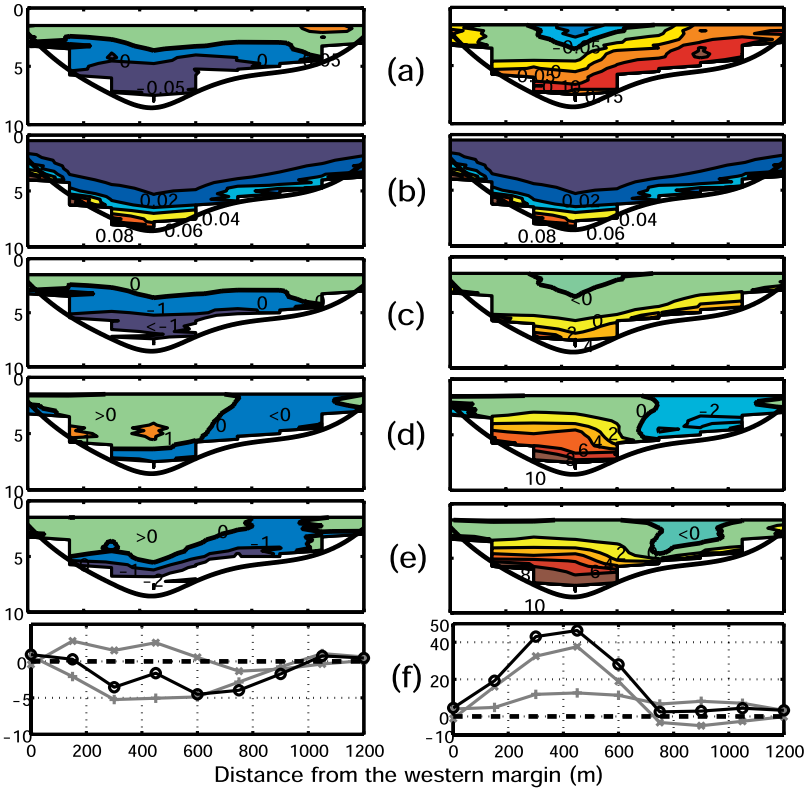

Figure 6. Tidally averaged vector quantities for the lateral and along-channel components (left and right column graphs, respectively). (a) Tidally averaged lateral velocity (contour units in m s^{-1}). (b) Tidally averaged suspended sediment concentration (units in kg m^{-3}, same value for both the left and right, concentration is a scalar). (c) Residual advective flux (in g m^{-2} s^{-1}). (d) Oscillatory tidal flux (in g m^{-2} s^{-1}). (e) Total suspended sediment flux (in g m^{-2} s^{-1}). (f) Depth-integrated sediment fluxes for residual advective flux (gray line with plus sign), oscillatory tidal flux (gray line with x sign) and total depth integrated sediment fluxes (black line with circles). Thick contour lines represent zero values while positive values represent flow or flux directed toward the east and/or up-estuary.

observed in mid-depth at the center of the channel. The western half of the cross-section, including the channel thalweg, is governed by eastward tidal fluxes, while the eastern half being composed of shallower regions is under a regime of westward directed tidal fluxes (Figure 6d). Thus the tidal oscillating component of sediment fluxes converges near the boundary between the main channel and the western shoal.

[28] The total net fluxes, defined as the sum of the residual advective and tidal fluxes, show the characteristics of a two-layered sediment transport pattern. A net eastward-directed flux is observed in the surface layer of the western half section (Figure 6e). On the contrary, a westward net flux is observed at the bottom of the channel and the whole water column on the eastern shoal (Figure 6e), which supplies sediments from the shoal to the channel. This creates a clockwise lateral circulation pattern in total sediment fluxes during a tidal cycle, and also strong convergence between opposite directed fluxes. The convergence plane extends from the bottom of the western shoal through the mid depth in the channel to the surface layer on the eastern shoal (Figure 6e). The depth-integrated total fluxes are generally directed to the west and their magnitude decreases near the center of the channel and the western shoal (Figure 6f), suggesting local supply of laterally transported sediment which is redistributed by the along-channel flow.

3.3.2. Lateral Variability of Along-Channel Sediment Transport

[29] The lateral variability of along-channel sediment flux is also estimated along transect A using equation (1) after substituting the lateral velocity (V) with the along-channel velocity (U). Along-channel residual advective flux in the channel is directed seaward and landward in the surface and bottom layers, respectively (Figure 6c), which is consistent with the pattern of residual flow observed by *Kim and Voulgaris* [2005] using different data set to estimate along-channel variability of residual circulation. On both shoals however only up-estuary directed fluxes are observed. Depth-integrated residual advective fluxes are directed up-estuary for the whole cross section (Figure 6f). The pattern of oscillatory tidal flux is divided horizontally into two sections: channel versus eastern shoal. While strong landward fluxes dominate the channel section, fluxes on the eastern shoal are directed seaward (Figure 6d). The maximum magnitude of tidal fluxes is approximately twice larger than that of

residual advective fluxes with the former defining the pattern of total fluxes (Figures 6e and 6f).

4. Discussion

4.1. Cross-Channel Momentum Balance Analysis

[30] In order to estimate the main forces involved in generating the lateral flows we observed in the curved, stratified estuarine channel, the lateral momentum balance along transect A is examined. The cross-channel momentum balance equation for a stratified flow in a curved channel can be written in curvilinear coordinates as [*Kalkwijk and Booij*, 1986; *Geyer*, 1993; *Chant and Wilson*, 1997; *Lacy and Monismith*, 2001]:

$$\frac{\partial v}{\partial t}+u\cdot\frac{\partial v}{\partial s}+\frac{u^2}{R_s}-f\cdot u+g\cdot\frac{\partial \eta}{\partial n}+\frac{g}{\rho_0}\cdot\frac{\partial}{\partial n}\cdot\int_z^0\rho(z')dz'-\frac{\partial}{\partial z}\left(A_z\frac{\partial v}{\partial z}\right)=0 \quad (2)$$

where s, n, and z are the along-, cross-channel and vertical coordinates, u and v are the horizontal velocity components in the s and n directions. A_z is the eddy viscosity, R_s is the radius of curvature, f is the Coriolis parameter, g is the gravitational acceleration, η is the water level, ρ is the density of the water and ρ_0 is the mean density. The positive sign in s, n and z represent up-estuary, eastward (i.e., rightward when looking up-estuary), and downward directions, respectively. Using characteristic values for the study area ($u \approx 0.7$ m s^{-1}, $v \approx 0.1$ m s^{-1}, $z \approx 10$ m, $R_s \approx 3000$ m, $f \approx 8.8 \times 10^{-5}$ s^{-1}, $\frac{\partial v}{\partial t} \approx 2 \times 10^{-5}$ m s^{-2}, $\frac{\partial v}{\partial s} \approx 10^{-5}$ s^{-1}, $\frac{\partial \eta}{\partial n} \approx 1 \times 10^{-5}$, $\rho_0 \approx 1005$ kg m^{-3}, $\frac{\partial}{\partial n}\cdot\int_z^0\rho(z')dz' \approx 10^{-2}$ kg m^{-3}, $A_z \approx 2 \times 10^{-3}$ m s^{-2} and $\frac{\partial v}{\partial z} \approx 10^{-2}$ s^{-1}, see *Kim and Voulgaris* [2005] and *Kim* [2006] for details), a scaling analysis shows that the advective acceleration term ($u\cdot\frac{\partial v}{\partial s}$) is more than one order of magnitude smaller than the other terms, and therefore can be eliminated (see also *Kalkwijk and Booij* [1986] and *Lacy et al.* [2003]), so that equation (2) reduces to:

$$\frac{\partial v}{\partial t}+\frac{u^2}{R_s}-f\cdot u+g\cdot\frac{\partial \eta}{\partial n}+\frac{g}{\rho_0}\cdot\frac{\partial}{\partial n}\cdot\int_z^0\rho(z')dz'-\frac{\partial}{\partial z}\left(A_z\frac{\partial v}{\partial z}\right)=0 \quad (3)$$

where the first term is the local acceleration of the lateral flow (AC). The second, third and fifth terms are the centrifugal forcing (CT), Coriolis acceleration (CF) and the lateral baroclinic pressure gradient (BC), respectively, while lateral pressure gradient is represented by the fourth term. The last term represents vertical frictional dissipation (FD). After vertically averaging and assuming that the depth-averaged lateral flow is zero, equation (3) becomes:

$$\frac{\overline{u^2}}{R_s}-f\cdot\overline{u}+g\cdot\frac{\partial \eta}{\partial n}+\overline{\frac{g}{\rho_0}\cdot\frac{\partial}{\partial n}\cdot\int_z^0\rho(z')dz'}-\overline{\frac{\partial}{\partial z}\left(A_z\frac{\partial v}{\partial z}\right)}=0 \quad (4)$$

where the overbar denotes vertically averaged values. By subtracting equation (4) from (3) and rearranging the terms, we obtain the following equation that describes lateral circulation:

$$\frac{\partial v}{\partial t}=-\frac{\left(u^2-\overline{u^2}\right)}{R_s}+f\cdot(u-\overline{u})-\frac{g}{\rho_0}\cdot\left(\frac{\partial}{\partial n}\cdot\int_z^0\rho(z')dz'-\overline{\frac{\partial}{\partial n}\cdot\int_z^0\rho(z')dz'}\right)+\left(\frac{\partial}{\partial z}\left(A_z\frac{\partial v}{\partial z}\right)-\overline{\frac{\partial}{\partial z}\left(A_z\frac{\partial v}{\partial z}\right)}\right) \quad (5)$$

[31] Note that the barotropic effect, represented by the term ($g\cdot\frac{\partial \eta}{\partial n}$) in equations (3) and (4), is removed in equation (5) because barotropic forcing is same everywhere in the vertical direction. The above equation states that in a curved channel and under stratified conditions, the acceleration of the lateral flow (AC) is controlled by the forcing induced by the sum of centrifugal acceleration, Coriolis force and lateral baroclinic pressure gradient (CT + CF + BC) and the frictional dissipation (FD).

[32] The temporal variability of the terms shown in equation (5) is calculated for a complete tidal cycle (i.e., 12.5 hours) and the results are shown in Figure 7. The current data collected in station A_1 were used to estimate the centrifugal and Coriolis force terms, while forward differentiating was utilized to calculate the acceleration term (see Appendix for details). Hydrographic data from the stations located west and east of station A_1 (220 m and 660 m from the western margin, respectively; see Figure 1 for location) were used in deriving the lateral baroclinic pressure gradient values. Thus the results shown in Figure 7 represent the intratidal variability of each momentum term within the channel. The average uncertainty in the values of AC, CT, CF and BC is 6.60×10^{-6}, 6.21×10^{-6}, 1.73×10^{-6} and 8.50×10^{-6} m s^{-2}, respectively (see Appendix). The difference between acceleration (AC) and the sum of three forcings (CT + CF + BC) represents a residual that consists of the sum of frictional dissipation (FD), any nonlocal forcing and measurement error. At this juncture, we should mention that no vertical eddy viscosity values were estimated using equation (5), as the uncertainty of the estimates was comparable to the expected magnitude of the term itself ($O(10^{-3}$ m s$^{-2})$). Nevertheless, the value of the term we obtained was similar to that obtained if we assume a typical vertical eddy viscosity of 2×10^{-3} m s^{-2} (e.g., *Kim and Voulgaris*, 2005) indicating that our analysis and approximations were reasonable and within the acceptable levels of confidence for natural systems.

[33] During ebb (1 to 6 hours), the along-channel flow is stronger at the surface layer, which leads to the development of a centrifugal force, $-\frac{u^2-\overline{u^2}}{R_s}$, directed toward the outside of the curvature (i.e., westward in the cross-section that is represented by negative values; Figure 7b). This causes accumulation of water mass toward the outside of the curved channel; this in turn drives a return flow in deeper parts of the channel which is shown as an opposite-directed centrifugal forcing (i.e., toward the inside of the curvature

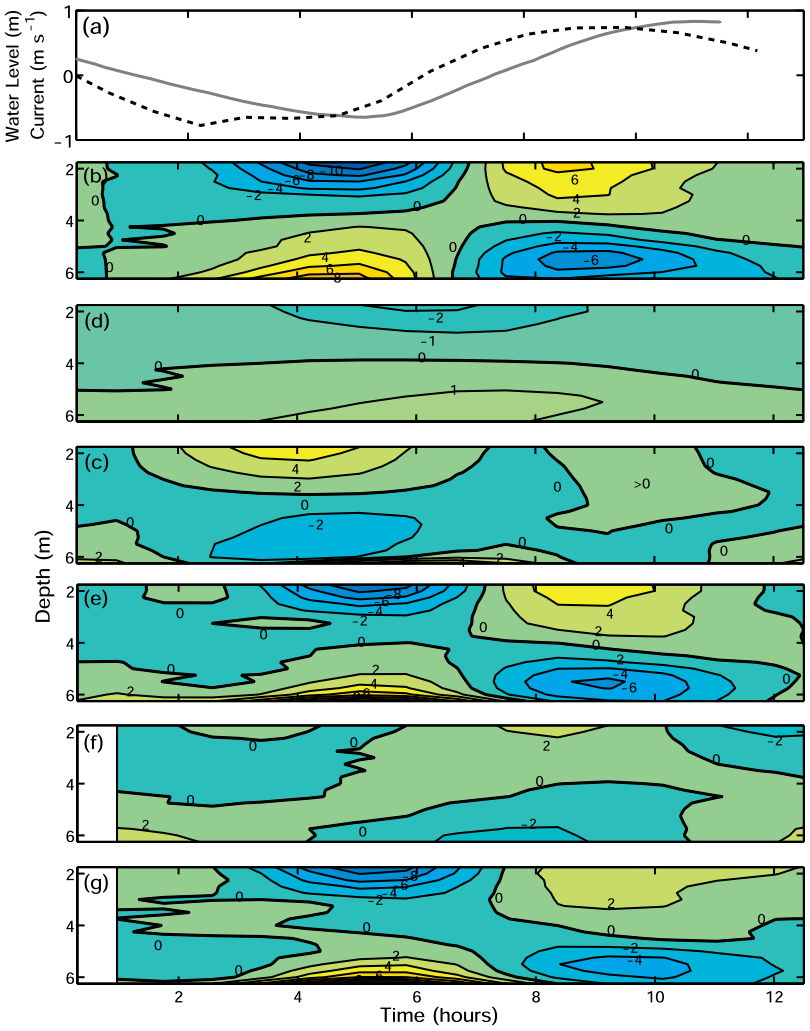

Figure 7. Time series of (a) water level (in m) and depth-averaged along-channel current (in m s^{-1}), (b) centrifugal forcing, (c) cross-channel baroclinic forcing, (d) Coriolis acceleration, (e) sum of these three forcings (right side of equation 5), (f) acceleration and (g) residual term that includes frictional dissipation, non-local forcing and measurement error. Contour units in $\times 10^{-5}$ m s^{-2}.

or eastward). This process contributes to the development of a counterclockwise lateral circulation when looking up-estuary (Figure 7b). Coriolis forcing ($f \cdot (u - \overline{u})$) is directed westward and eastward in the surface and bottom layers, respectively (Figure 7d), but its magnitude is approximately 80% smaller than that of the centrifugal acceleration term. The dominance of the centrifugal acceleration over the Coriolis force is also confirmed by the large Rossby number ($u/(R_x \cdot f)$), which is 5.33 for the study area. During early ebb (hours 2 to 3) differential advection leads to a lateral inclination of the isohalines (see Figure 4 and section 3.2.2) and thus the generation of a strong lateral baroclinic pressure gradient [e.g., *Dronkers*, 1996; *Chant and Wilson*, 1997; *Lacy and Monismith*, 2001, *Lacy et al.*, 2003], with a direction opposite to that of the centrifugal acceleration (Figure 7c). Since centrifugal forcing is relatively weak because of slower along-channel velocity during early ebb, the interaction between centrifugal, lateral baroclinic and Coriolis forcings results in a weak acceleration and leads to the generation of a three-layer lateral acceleration: eastward, westward and eastward in the surface, middle and bottom water layers, respectively (Figure 8c). A similar weak, three layer, lateral flow system has been identified in the Hudson River estuary, under stratified conditions (see Figure 15 in *Lerczak and Geyer* [2004]). After this period the centrifugal forcing term increases and dominates over the opposite-directed lateral baroclinic forcing in driving lateral flows during maximum and late ebb (Figures 7b and 7c). Such a temporal variation in lateral circulation pattern even during a tidal phase was also reported in Snag Channel by *Lacy and Monismith* [2001]. During mid to late ebb (hours 4 to 7), the residuals, represented by the difference between the total forcing and acceleration show relatively larger values (Figure 7g). Although not clear at present, this might be due to the fact that the transect is located just upstream of the strong curvature during ebb, which results in the influence of nonlocal forcings at the transect rather than the curvature effect.

[34] During flood the maximum along-channel velocity is observed at mid-depth (see Figure 5a) and decreases both toward the sea surface and the bed. This subsurface maximum velocity layer (see Figure 5), a common feature of

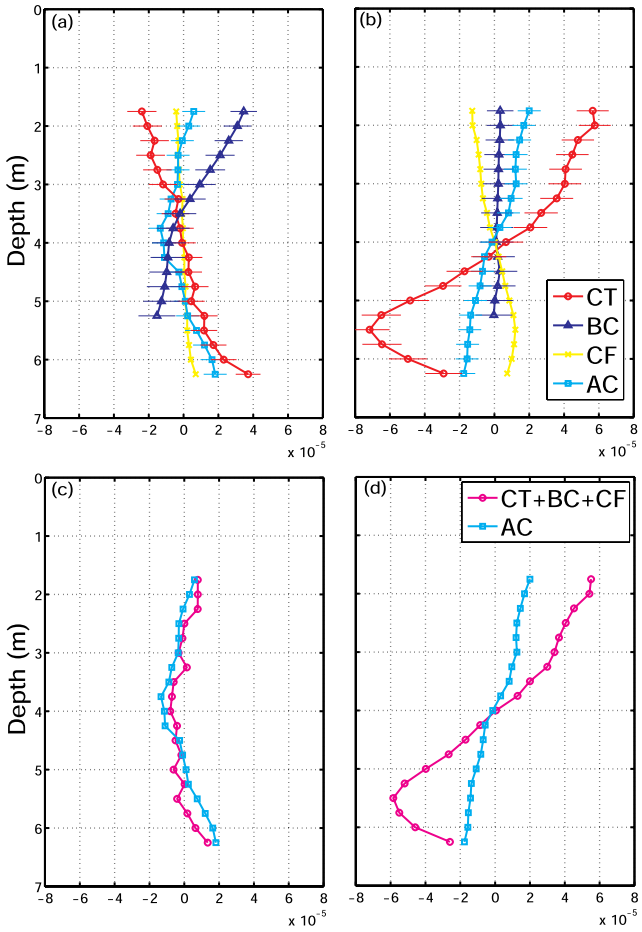

Figure 8. Vertical variation of the lateral momentum terms during early stage of ebb (hour 3; a and c) and maximum flood (hour 9.2; b and d). Black lines represent the terms in the right side of equation 5; centrifugal acceleration (CT), Coriolis forcing (CF) and baroclinic pressure gradient (BC). Gray lines represent acceleration (AC) term in equation 5. Uncertainty calculation for error bars are shown in Appendix.

estuarine environments during flood [e.g., *Jay and Musiak*, 1994; *Lacy and Monismith*, 2001; *Lacy et al.*, 2003], leads to the development of a westward-directed centrifugal forcing in the mid-to-bottom layer. The associated Coriolis forcing is directed westward and eastward in the surface and bottom layers, respectively (Figure 7d) and its magnitude is approximately 70–80% smaller than that of the centrifugal force. Also, the isohalines are more or less horizontal during flood (see Figure 5c), suggesting a minimal or no contribution of lateral baroclinicity to lateral circulation (see hours 8 to 12; Figure 7c). Thus centrifugal forcing appears to be the dominant term that drives a relatively strong clockwise circulation during the early and mid stages of flood. This is clearly shown in Figures 8b and 8d which show the vertical variability of the lateral momentum balance at maximum flood (hour 9.2). The centrifugal forcing during flood appears to contribute to the generation of a relatively strong clockwise-directed force (Figure 8b). The lateral flow acceleration term shows also clockwise circulation during maximum flood, which indicates same direction as those of the sum of three forcing terms (Figure 8d). Note that the magnitude of each term is larger during flood than ebb (Figures 8c and 8d), which is consistent with the results of stronger lateral currents during flood.

4.2. Driving Forces for Lateral Circulation

[35] The momentum analysis presented in section 4.1 showed that the magnitude of centrifugal forcing (up to 1×10^{-4} m s^{-2} m s^{-2}) is relatively larger than the sum of Coriolis and lateral baroclinic forcings during both flood and ebb, except for the period of early ebb (Figures 7 and 8). Thus the channel curvature appears to control the generation of lateral circulation throughout much of the tidal cycle. In contrast to our findings, lateral circulation patterns in the Hudson River estuary [*Chant and Wilson*, 1997] and San Francisco Bay [*Lacy and Monismith*, 2001] are controlled by the time-varying balance between centrifugal forcing and lateral baroclinic pressure gradient. In the Hudson River case, the magnitude of centrifugal forcing is approximately 3 times smaller than that found in this study, which can be explained by the difference in curvature radius between the two systems (i.e., the radius of curvature at the headland of Hudson is the order of 10 km which is roughly 3 times larger than that of channel curvature in Winyah Bay). On the other hand, Snag Channel (San Francisco Bay) has a radius of 920 m [*Lacy and Monismith*, 2001] which is 3 times smaller than that of Winyah Bay (3000 m). In Snag Channel however the maximum current speed does not exceed 0.6 m s^{-1}, which is half the magnitude of the speeds measured in this study. A simple comparison of the magnitudes of the centrifugal forcing shows that in Winyah Bay centrifugal forcing is 4/3 times larger than that reported for Snag Channel. Thus the increased centrifugal forcing due to high curvature radius and strength of downstream velocity dominates lateral circulation patterns in Winyah bay when compare to other natural systems.

[36] Another significant characteristic of the observed lateral flow pattern is the tidal asymmetry, with stronger lateral flows during flood than ebb (see Figures 4 and 5). This is attributed to the increased values of the dominant forcing momentum terms which are almost 3 times larger during maximum flood than ebb (Figures 8c and 8d). This asymmetry is similar to that observed in the Hudson river [*Lerczak and Geyer*, 2004] with 4 times stronger lateral currents during flood and ebb. On the other hand, the present asymmetry pattern is opposite to that found in Snag Channel where the lateral circulation was stronger and more consistent during ebb than flood [*Lacy and Monismith*, 2001]. Overall the type of asymmetry observed depends on the relative importance and signs of the centrifugal and lateral baroclinic forcing terms [c.f., *Lacy and Monismith*, 2001]. Even though the centrifugal acceleration can be the dominant forcing, a competing lateral baroclinic pressure gradient can reduce the total forcing driving lateral circulation in our study area. During ebb, for example, counterclockwise centrifugal acceleration (west- and east-directed forcing in surface and bottom layer, respectively; Figures 7b and 8a) is canceled out by the opposite-directed lateral baroclinic forcing leading to the occurrence of a weak secondary circulation (Figures 7 and 8). Furthermore, relatively stronger lateral baroclinic pressure gradient due

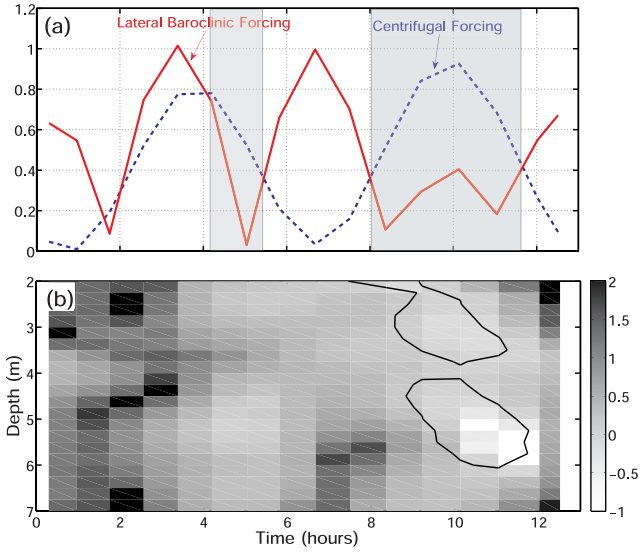

Figure 9. (a) Temporal variability of the centrifugal (dashed) and the lateral baroclinic (solid) forcing terms in equation (6) (in $\times 10^{-4}$ m s^{-2}). Shaded areas represent the period when the centrifugal acceleration dominates over the lateral baroclinic forcing. (b) Temporal and vertical variability of the gradient Richardson number ($Ri = -\frac{\rho_0}{g} \cdot \frac{d\rho}{dz} \cdot (\frac{du}{dz})^{-2}$) estimated using the data from station A_1. Values shown are $\log_{10}(Ri/0.25)$, so the positive and negative values represent stratified and well-mixed conditions, respectively. Thick contour lines correspond to $Ri = 0.25$ and the insides of the contours represent $Ri < 0.25$.

to differential along-channel advection can result in a near-balance between centrifugal forcing and baroclinic pressure gradient (Figures 7b, 7c, and 8a). On the other hand, during flood lateral circulation is dominated by the centrifugal forcing since the isohalines are mostly horizontal (Figure 5), which results in relatively weak lateral baroclinic pressure gradient.

[37] *Seim and Gregg* [1997] suggested a criterion for evaluating the relative importance between lateral stratification and centrifugal forcing. According to their work, given an inviscid flow, a balance between centrifugal forcing and lateral baroclinic pressure gradient is assumed and the lateral momentum balance equation (5) is scaled as,

$$\frac{\alpha \cdot \overline{u^2}}{R_s} = \frac{g}{\rho_0} \cdot \frac{\Delta\rho}{B} \cdot h \qquad (6)$$

where $\alpha = (u^2 - \overline{u^2})/\overline{u^2}$, $\Delta\rho$ is density difference across the channel with width, B, and h is the water depth. According to (6) when the along-channel velocity is stronger than a critical value, the centrifugal acceleration would be strong enough to overturn the stratification and thus a well-mixed condition occurs in the downstream of the curvature. In *Seim and Gregg* [1997] it is assumed that lateral stratification can take the same value as the vertical stratification upstream of the channel curved section. This assumption requires a 90 degree tilting of the isohalines within the curved section. However this can only occur when centrifugal forcing is strong (high along-channel velocity and/or small curvature radius) and if there is enough time for the tilting to occur (i.e., small along-channel speed). These requirements are difficult to be satisfied in natural systems, as it was the case in *Lacy and Monismith* [2001]. This scaling even failed to predict the flow in point Defiance, in *Seim and Gregg* [1997], although this was attributed to the geometry of the channel (see page 3467 in *Seim and Gregg* [1997]). Applying the criterion to our study site, we find that lateral baroclinic force is larger than centrifugal forcing during early ebb and every slack period, while centrifugal force dominates over baroclinic force during late stage of ebb and most of flood (shaded areas in Figure 9a). However relatively stronger centrifugal forcing during flood is not indicative of the capacity of the centrifugal acceleration to overturn the density field as suggested by *Seim and Gregg* [1997]. There is no significant relationship between stratification and lateral circulation pattern in our data and as shown by the gradient Richardson number from the station A_1; for example, the water column was stratified during early flood (hours 6–9) and well-mixed during late flood (hours 9–12; Figure 9b), while the lateral flow is quite strong for the whole period of flood (Figure 2d) regardless of stratification. Thus our analysis supports the conclusions of *Lacy and Monismith* [2001, see page 31,300] that the criterion shown in equation (6) might not be a reliable for natural systems, as the balance between centrifugal acceleration and lateral baroclinic forcing requires time to develop. In natural systems, lateral baroclinic forcing might be dominated by differential downstream advection rather than tilting of the isohalines because of the centrifugal forcing. Furthermore, the geometry of the channel (wider channel in Winyah Bay, versus narrow channels in the *Seim and Gregg* [1997] work) might contribute to the criterion failing to describe lateral circulation patterns.

4.3. Implication on Sediment Transport

[38] The pattern of landward-directed fluxes observed in the center of the channel shown in Figure 6 are consistent with the results presented in *Goñi et al.* [2005] who calculated sediment flux using a conventional water sampling method. Thus the landward transport of suspended sediments can result in siltation of the main navigation channel in the upper part of the estuary. This is confirmed by the regular dredging required to take place in the study area [*USACE*, 1997]. Such landward movement of sediments, mostly by tidal pumping processes, is consistent with the results from the Hudson River estuary reported by *Geyer et al.* [2001] and supports the idea of *Meade* [1969] that estuaries tend to import sediment from the seaward direction.

[39] Although the along-channel transport of suspended sediments is the dominant process in understanding the development and evolution of sediment transport processes in estuaries, cross-channel variations of sediment distribution can also be important [e.g., *Geyer et al.*, 1998]. The relative importance between along- and cross-channel sediment transport can be evaluated by comparing the advection term in along-channel ($u \cdot \partial c/\partial s$) and lateral ($v \cdot \partial c/\partial n$) direction. The magnitude of lateral flows (v) is generally one order smaller than that of the along-channel flow (u), which is consistent with our results for the study area. However our data show the lateral gradient of depth-averaged concentration of suspended sediments ($\partial\bar{c}/\partial n$) a maximum

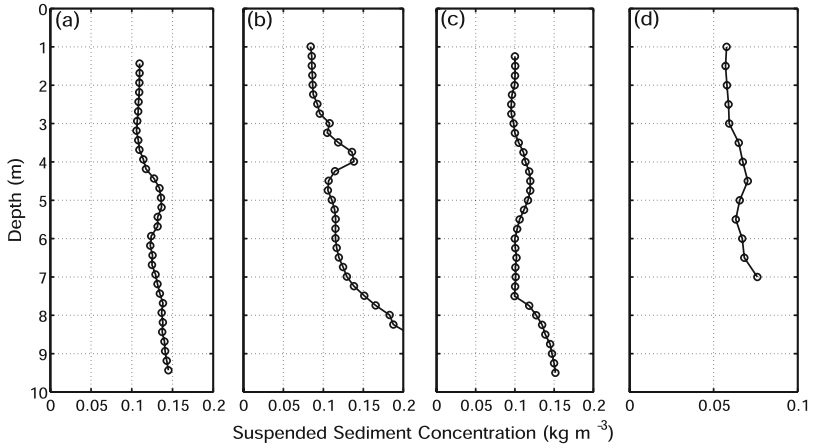

Figure 10. Vertical profiles of suspended sediment concentration observed in the vicinity of the estuarine turbidity maximum of Winyah Bay during (a) flood at October 2001, (b) ebb at May 2002, (c) flood at September 2002 and (d) flood at March 2005. The data were collected by an OBS and then calibrated with in-situ pumped water sample. Note different horizontal scale in (d).

of 7.3×10^{-4} kg m^{-4}, which is two orders of magnitude larger than the along-channel gradient ($\sim 10^{-6}$ kg m^{-4}; see *Kim* [2006]). This suggests that the contribution of lateral sediment transport is at least as significant as that in the along-channel direction in controlling sedimentary processes. This is further reinforced by the mid-depth layer of elevated sediment concentration that usually appears in the profiles obtained at the center of the channel (see Figures 2 and 5). These layers are also observed at numerous stations in the vicinity of turbidity maximum zone during other cruises (see Figure 10). The depths of both the western shoal and the bottom of the eastward-directed flow layer (see Figure 5b) correspond to that of the observed mid-water local concentration maxima suggesting lateral advection of sediment.

[40] Numerical simulations for the Hudson River estuary showed that lateral sediment transport may cause net trapping of sediments on the region of the shoal [*Geyer et al.*, 1998]. In contrast, this study shows that the convergence zone in net sediment fluxes is observed in the vicinity of the boundary between the central channel and the western shoal (Figure 6). This finding is in agreement with results presented from the upper Chesapeake Bay that the convergence zone of lateral sediment flux occurs in the vicinity of the boundary between estuarine channel and a shoal with relatively steep slope (see Figure 13 of *Fugate et al.* [2007]). Figure 6c also shows that sediments near the bed were advected from the eastern shoal to the channel. A decrease of sediment flux rate in the center of the channel also suggests that trapping of suspended sediments occurs. This is believed to be one of the main mechanisms for the development of the estuarine turbidity maximum at this location. The location of turbidity maximum is generally associated with the freshwater–saltwater interface zone [e.g., *Uncles et al.*, 1998, 2006; *Kistner and Pettigrew*, 2001; *Sanford et al.*, 2001]. However the turbidity maximum in Winyah Bay is developed in the vicinity of transect A which is 10 km downstream of the freshwater–saltwater interface [*Ramsey*, 2000; *Kim and Voulgaris*, 2003, *Goñi et al.*, 2005; *Kim*, 2006]. Muddy deposits are prevalent even in the channel near transect A, while the channel beds in most of middle and lower part of the estuary are composed of sandy deposits [*White et al.*, 2003], which also confirms the fact that the fine sediments on the shoal are advected to the channel.

[41] Traditional lateral sediment transport in a curved open channel (i.e., river bend, see *Allen* [1970], *Bridge and Jarvis* [1982]) demands that the helical flow, induced by the centrifugal forcing, intensifies meandering by eroding the outer channel wall and creating a bank on the inside of the bend. However this study shows that in a partially mixed estuarine curved channel, a different sediment transport pattern can occur; sediments are transported from the shoal on the inner bend to the center of the channel in response to tidal and baroclinic forcings. An investigation on historical change of the study area using old maps has shown that there is no significant changes in morphology near the channel bend during last 150 years, with the exception of the presence of an island that was created artificially by dumping dredged material. This leads us to hypothesize that observed lateral sediment transport pattern prevents the build-up of the inside shoal and mitigates some of the erosion on the outside, thus maintaining the curvature observed, and up to a degree creating a morphological equilibrium state. Although this is not definite at present, it deserves further investigation by examining a larger number of curved estuarine channels which is beyond the scope of the present study.

5. Conclusions

[42] Our analysis indicates that both the development of lateral circulation and distribution of fine sediment are strongly related to the curvature of the estuarine channel in conjunction with the effect of vertical stratification. During ebb, centrifugal forcing drives movement to the outside and inside of the curve in the surface and bottom layers, respectively, creating a counterclockwise lateral circulation pattern (when looking up-estuary) in an eastward curved section. Interaction between this centrifugal forcing

and opposing-directed lateral baroclinic pressure gradient induced by differential advection, results in weak lateral flows during this period. On the other hand, opposing (i.e., clockwise) centrifugal forcing is developed during flood because of maximum along-channel current layer present at mid-depth. Lateral stratification during this period produces a relatively weak baroclinic pressure gradient in clockwise direction, which also reinforces the development of lateral flows.

[43] The pattern of lateral currents seems to control the lateral transport of suspended sediments. An observed mid-depth layer with elevated sediment concentrations coincides with the depth of eastward-directed lateral currents. This implies that the fine sediments resuspended from the shoal bed were delivered to the center of the channel by the lateral currents. The tidally averaged sediment fluxes showed that net convergence of suspended sediments occurred at the western boundary of the central channel. Sediments near the bed are advected from the broad, gentle eastern shoal to the channel and might be entrapped on the center and western part of the channel. This could be related to the development of ETM at a curved section of the estuarine channel, and potentially explains the limited meandering of the estuarine channel in the study area.

Appendix A: Uncertainty Analysis

[44] In the estimation of the errors for the lateral momentum balance terms presented in the manuscript we followed a similar method as that described in *Lacy and Monismith* [2001] and the results of the uncertainty analysis are presented below.

[45] In the post-cruise processing of the collected ADCP data, current velocities were averaged over the period of required for the completion of a CTD cast (approximately 90 seconds), which correspond to 90 ensembles. The total per-ensemble uncertainty was estimated as the standard deviation of the 90 measurements. The mean standard deviation for 1401 average values of the along-channel velocity from 90 measurements is 15.2 cm s^{-1}, while for the cross-channel velocity is 13.9 cm s^{-1}. The uncertainties in the spatially averaged values are 1.6 and 1.4 cm s^{-1} for the u and v components, respectively.

[46] The salinity and sediment concentration values shown were obtained from the vertical profiles of the CTD and OBS casts. The collected data were spatially averaged over distances equal to the ADCP bin size (25 cm), which corresponded to averaging approximately 6 instantaneous cast measurements. The mean standard deviation for 1406 averaged values of density is 0.069 kg m^{-3}, and thus the standard error in water density estimates is 0.028 kg m^{-3}.

[47] The uncertainty in centrifugal acceleration (σ_{CT}) estimates is calculated as (see *Lacy and Monismith* [2001])

$$\sigma_{CT} = \frac{1}{R_x} \cdot \sqrt{4 \cdot \sigma_u^2 \cdot \left(\frac{\overline{u^2}}{N} + u^2 \right) + (CT \cdot \sigma_{R_s})} \qquad \text{(A1)}$$

where σ_u is estimated above to be 0.016 m s^{-1}, and σ_{Rs} is 100 m. The average uncertainty, σ_{CT}, for the results shown in Figure 7 is 6.21 $\times$ 10^{-6} m s^{-2}, and the maximum is 1.18 $\times$ 10^{-5} m s^{-2}.

[48] The uncertainty in estimating lateral baroclinic pressure gradient (σ_{BC}) is calculated using:

$$\sigma_{BC} = \sqrt{2} \cdot \frac{g}{\rho_0 \cdot \Delta_i} \cdot \sigma_\rho \sqrt{i + \frac{N+1}{2}} \qquad \text{(A2)}$$

where, i is the index of the depth cell, σ_ρ is estimated at 0.028 kg m^{-3} (see above), N = 19 (the number of depth cells at station 3 stations, A_1, A_2 and east of A_1 in Figure 1), and ΔN is 200 m. The estimate of σ_{BC} ranges from 0.65 $\times$ 10^{-5} m s^{-2} near the surface to 1.06 $\times$ 10^{-5} m s^{-2} near the bed.

[49] The uncertainty in calculating Coriolis forcing was estimated as

$$\sigma_{CF} = f \cdot \left(\sigma_u + \frac{\sigma_u}{N} \right) \qquad \text{(A3)}$$

where σ_u is estimated at 0.016 m s^{-1} above and N is 19. With these values σ_{CF} was found to be 1.73 $\times$ 10^{-6} m s^{-2}.

[50] Acceleration in the cross-channel velocity was calculated from the data using forward differencing as

$$AC = \frac{v_j - v_{j-1}}{\Delta t} \qquad \text{(A4)}$$

except at the first measurement. The uncertainty in $\Delta v = v_j - v_{j-1}$ is $\sqrt{2}\sigma_v$ and the uncertainty in estimating acceleration is as

$$\sigma_{AC} = \frac{\sqrt{2}\sigma_v}{\Delta t} \qquad \text{(A5)}$$

where σ_v is estimated at 0.014 m s^{-1} and Δt is approximately 3000 seconds. Thus the uncertainty σ_{AC} is 6.60 $\times$ 10^{-6} m s^{-2}.

[51] **Acknowledgments.** The authors would like to thank the two anonymous reviewers for their comments and helpful suggestions. Dr. L. Sanford is thanked for his helpful comments on early draft of this paper. The data collection work was supported by the Environmental Protection Agency/EPSCoR grant No. R-82942401-O. Ship time on board the R/V Ferrel was provided by the National Ocean and Atmosphere Administration (NOAA) through the National Estuarine Research Reserve System (NERRS) program. Support during the data analysis and preparation of this manuscript was provided by NOAA (Award NA04OAR43100099). Additional support for G. Voulgaris was provided by the National Science Foundation (Awards: OCE-0451989 and OCE-0535893).

References

Allen, G. P., J. C. Salomon, P. Bassoullet, Y. du Penhoat, and C. de Grandpre (1980), Effects of tides on mixing and suspended sediment transport in macrotidal estuaries, *Sediment. Geol.*, *26*, 69–90.

Allen, J. R. L. (1970), A quantitative model of grain size and sedimentary structures in lateral deposits, *Geol. J.*, *7*, 129–146.

Blake, A. C., G. C. Kineke, G. G. Milligan, and C. R. Alexander (2001), Sediment trapping and transport in the ACE Basin, South Carolina, *Estuaries*, *24*, 721–733.

Bridge, J. S., and J. Jarvis (1982), The dynamics of a river bend: a study in flow and sedimentary processes, *Sedimentology*, *29*, 499–541.

Chant, R. J. (2002), Secondary circulation in a region of flow curvature: Relationship with tidal forcing and river discharge, *J. Geophys. Res.*, *107*(C9), 3131, doi:10.1029/2001JC001802.

Chant, R. J., and R. E. Wilson (1997), Secondary circulation in a highly stratified estuary, *J. Geophys. Res.*, *102*, 23,207–23,215.

Dronkers, J. (1996), The influence of buoyancy on transverse circulation and on estuarine dynamics, in *Buoyancy Effects on Coastal and Estuarine Dynamics*, edited by D. G. Aubrey and C. T. Friedrichs, pp. 341–356, AGU, Washington, D. C.

Dyer, K. R. (1986), *Coastal and Estuarine Sediment Dynamics*, 342 pp, John Wiley and Sons, New York.

Friedrichs, C. T., B. A. Armbrust, and de H. E. Swart (1998), Hydrodynamics and equilibrium sediment dynamics of shallow, funnel-shaped tidal estuaries, in *Physics of Estuaries and Coastal Seas*, edited by J. M. Dronkers and B. A. M. Scheffers, pp. 315–328, Balkema Press, Rotterdam, Netherlands.

Fugate, D. C., C. T. Friedrichs, and L. P. Sanford (2007), Lateral dynamics and associated transport of sediment in the upper reaches of a partially mixed estuary, Chesapeake Bay, USA, *Cont. Shelf Res.*, *27*, 679–698.

Geyer, W. R. (1993), Three-dimensional tidal flow around headlands, *J. Geophys. Res.*, *98*, 955–966.

Geyer, W. R., R. P. Signell, and G. C. Kineke (1998), Lateral trapping of sediment in a partially mixed estuary, in *Physics of Estuaries and Coastal Seas*, edited by J. M. Dronkers and B. A. M. Scheffers, pp. 115–124.

Geyer, W. R., J. D. Woodruff, and P. Traykovski (2001), Sediment transport and trapping in the Hudson River estuary, *Estuaries*, *24*, 670–679.

Goñi, M. A., M. W. Cathey, Y. H. Kim, and G. Voulgaris (2005), Fluxes and sources of suspended organic matter in an estuarine turbidity maximum region during low discharge conditions, *Estuarine Coastal Shelf Sci.*, *63*, 683–700.

Grabemann, I., and G. Krause (1989), Transport processes of suspended matter derived from time series in a tidal estuary, *J. Geophys. Res.*, *94*, 14,373–14,379.

Huijts, K. M. H., H. M. Schuttelaars, H. E. de Swart, and A. Valle-Levinson (2006), Lateral trapping of sediment in tidal estuaries: An idealized model study, *J. Geophys. Res.*, *111*, C12016, doi:10.1029/2006JC003615.

Jay, D. A., and J. D. Musiak (1994), Particle trapping in estuarine tidal flows, *J. Geophys. Res.*, *99*, 445–461.

Kalkwijk, J. P. T., and R. Booij (1986), Adaptation of secondary flow in a nearly-horizontal flow, *J. Hydraul. Res.*, *24*, 19–37.

Kim, Y. H. (2006), Circulation and material transport in a partially stratified estuary: Winyah Bay, SC, Ph.D. thesis, 151 pp., Univ. of S. Carolina, Columbia.

Kim, Y. H., and G. Voulgaris (2003), Estimation of suspended sediment concentration in estuarine environments using acoustic backscatter from an ADCP, in *Proceedings of Coastal Sediments'03*, pp. 1–10, Clearwater Beach, FL.

Kim, Y. H., and G. Voulgaris (2005), Effect of channel bifurcation on residual estuarine circulation: Winyah Bay, South Carolina, *Estuarine Coastal Shelf Sci.*, *65*, 671–686.

Kistner, D. A., and N. R. Pettigrew (2001), A variable turbidity maximum in the Kennebec estuary, Maine, *Estuaries*, *24*, 680–687.

Lacy, J. R., and S. G. Monismith (2001), Secondary currents in a curved, stratified, estuarine channel, *J. Geophys. Res.*, *106*, 31,283–31,302.

Lacy, J. R., M. T. Stacey, J. R. Burau, and S. G. Monismith (2003), Interaction of lateral baroclinic forcing and turbulence in an estuary, *J. Geophys. Res.*, *108*(C3), 3089, doi:10.1029/2002JC001392.

Lerczak, J. A., and W. R. Geyer (2004), Modeling the lateral circulation in straight, stratified estuaries, *J. Phys. Oceanogr.*, *34*, 1410–1428.

Li, C. Y., and J. O'Donnell (1997), Tidally driven residual circulation in shallow estuaries with lateral depth variation, *J. Geophys. Res.*, *102*, 27,915–27,929.

Meade, R. H. (1969), Landward transport of bottom sediments of the Atlantic Coastal Plain, *J. Sed. Petrology*, *39*, 222–234.

Nichols, M. M., and R. B. Biggs (1985), Estuaries, in *Coastal Sedimentary Environments*, edited by R. A. Davis, pp. 77–186, Springer-Verlag, New York.

NOS (1995), Tide tables 1996: High and low water predictions, east coast of North and South America, including Greenland, 308 pp.

Nunes Vaz, R. A., and J. H. Simpson (1985), Axial convergence in a well-mixed estuary, *Estuarine Coastal Shelf Sci.*, *20*, 637–649.

Orton, P. M., and G. C. Kineke (2001), Comparing calculated and observed vertical suspended-sediment distributions from a Hudson River estuary turbidity maximum, *Estuarine Coastal Shelf Sci.*, *52*, 201–410.

Ott, M. W., and C. Garrett (1998), Frictional estuarine flow in Juan de Fuca Strait, with implications for secondary circulation, *J. Geophys. Res.*, *103*, 15,657–15,666.

Patchineelam, S. M. (1999), Fine-grained sediment dynamics and budget: Winyah Bay estuary, South Carolina, Ph.D. thesis, 190 pp., Univ. of S. Carolina, Columbia.

Ramsey, A. L. (2000), Physical processes controlling sediment transport in Winyah Bay, South Carolina, M.S. thesis, 137 pp., Boston college.

Sanford, L. P., S. E. Suttles, and J. P. Halka (2001), Reconsidering the physics of the Chesapeake Bay estuarine turbidity maximum, *Estuaries*, *24*, 655–669.

Seim, H. E., and M. C. Gregg (1997), The importance of aspiration and channel curvature in producing strong vertical mixing over a sill, *J. Geophys. Res.*, *102*, 3451–3472.

Smith, R. (1976), Longitudinal dispersion of a buoyant contaminant in a shallow channel, *J. Fluid Mech.*, *78*, 677–688.

Smith, R. (1980), Buoyancy effects upon longitudinal dispersion in wide well-mixed estuaries, *Proc. R. Soc. Ser. A*, *296*, 467–496.

South Carolina Sea Grant Consortium (1992), Characterization of the physical, chemical and biological conditions and trends in three South Carolina estuaries: 1970–1985, Winyah Bay and North Inlet estuaries, 117 pp.

USACE (1997), Dredged material management plan, preliminary assessment—Georgetown, SC. 66 pp.

Uncles, R. J., A. E. Easton, M. L. Griffiths, C. Harris, R. J. M. Howland, R. S. King, A. W. Morris, and D. H. Plummer (1998), Seasonality of the turbidity maximum in the Humber-Ouse Estuary, *Mar. Pollut. Bull.*, *37*, 206–215.

Uncles, R. J., J. A. Stephens, and C. Harris (2006), Runoff and tidal influences on the estuarine turbidity maximum of a highly turbid system: The upper Humber and Ouse Estuary, UK, *Mar. Geol.*, *235*, 213–228.

Valle-Levinson, A., K. C. Wong, and M. M. Lwiza (2000), Fortnightly variability in the transverse dynamics of a coastal plain estuary, *J. Geophys. Res.*, *105*, 3413–3424.

White, S., G. Voulgaris, and C. Amer (2003), Side-scan sonar characterization of sediments in Winyah Bay estuary, South Carolina, *Southeast Coastal Ocean Sciences Conference*, Charleston, SC.

Y. H. Kim, Horn Point Laboratory, University of Maryland Center for Environmental Science, PO Box 775, Cambridge, MD 21613, USA. (ykim@hpl.umces.edu)

G. Voulgaris, Department of Geological Sciences, Marine Science Program, University of South Carolina, Columbia, SC 29208, USA.